European Journal of Pharmaceutics and Biopharmaceutics 142 (2019) 421–434

Contents lists available at ScienceDirect

European Journal of Pharmaceutics and Biopharmaceutics

journal homepage: www.elsevier.com/locate/ejpb

Research paper

Bridging *in vitro* dissolution and *in vivo* exposure for acalabrutinib. Part I. Mechanistic modelling of drug product dissolution to derive a P-PSD for PBPK model input

Xavier J.H. Pepin[a,*], Natalie J. Sanderson[a], Alexander Blanazs[a], Shveta Grover[a], Timothy G. Ingallinera[b], James C. Mann[a]

[a] AstraZeneca, Pharmaceutical Technology and Development, Charter Way, Macclesfield SK10 2NA, UK
[b] Acerta Pharma, 121 Oyster Point Blvd. South San Francisco, CA 94080, USA[1]

ARTICLE INFO

Keywords:
Drug product
Dissolution
Mechanistic
Surface pH
Weak base
Prediction
Particle size
PBPK modelling

ABSTRACT

Drug product dissolution for four batches of acalabrutinib 100 mg capsules were analyzed with *in vitro* dissolution in various pH conditions and in media containing synthetic surfactant micelles or biorelevant micelles. Non-sink conditions, where the drug is unionized, were used to derive a batch specific drug product particle size distribution (P-PSD). The purpose of this P-PSD is to serve as an input in physiological based pharmacokinetic (PBPK) models to calculate *in vivo* dissolution in various administration conditions. The P-PSD was used to predict dissolution in all other conditions tested, introducing a different Unstirred Water Layer (UWL) thickness for free- and micelle-bound drug and the calculation of surface solubility using a theoretical model. With the proposed P-PSD approach and proposed model inputs, percent dissolved at all time points and for all conditions and batches were adequately anticipated with an 11% overprediction. In contrast, the use of drug substance laser diffraction particle size data with equivalent inputs to the models led to an underprediction of observed percent dissolved by 31% overall. Finally, the use of bulk solubility instead of surface solubility led to an overall 48% overprediction of the dissolution data. Batch specific P-PSD were used to predict *in vivo* dissolution of acalabrutinib drug products with PBPK models. The current limitations of PBPK models for integration of *in vitro* dissolution are also discussed and improvements are suggested to improve future predictions.

1. Introduction

Drug product batch dissolution data are used in the pharmaceutical industry in late stage development, to support important activities such as Quality by Design and the setting of clinically relevant specifications for the dissolution of the commercial product, or the particle size of the drug substance. Physiologically based pharmacokinetic models (PBPK) can bridge *in vitro* dissolution and *in vivo* absorption through the development of mechanistic *in vitro-in vivo* correlations. The approach to integration of drug product batch dissolution data in PBPK tools is currently a matter of debate, and best practices need to be derived for the industry and regulators [1,2]. In addition, other factors that can limit *in vivo* dissolution such as temperature or viscosity of the fluids [3], and the composition of the fluids if they react with the drug or the formulation, should be considered.

Calquence® (acalabrutinib) has received accelerated approval by the FDA for the treatment of adult patients with mantle cell lymphoma (MCL) who have received at least one prior therapy. Acalabrutinib is an amphoteric compound but can be treated as a diprotic base considering p*K*a values within the physiological pH range. Its dissolution and solubility are pH-dependent, and the use of PBPK models to calculate *in vivo* product dissolution should account for the impact of local pH at the surface of the crystal, and the effect of micelles and other diffusion limiting species if relevant to the dissolution process.

However, the way dissolution is handled currently in most commercial *in silico* PBPK software platforms, apart from GCoas v1.1 (Process Systems Enterprise Ltd), lacks certain key aspects of the dissolution process. These tools generally consider the bulk drug solubility as the main driver for dissolution rate and only account for diffusion of drug species from the surface, whether in free form or associated with micelles. In Simcyp v17 (Certara), the surface solubility is calculated for weak acids but not for weak bases, and in GastroPlus™ V9.0

* Corresponding author.
E-mail address: xavier.pepin@astrazeneca.com (X.J.H. Pepin).
[1] at the time of manuscript preparation.

https://doi.org/10.1016/j.ejpb.2019.07.014
Received 22 March 2019; Received in revised form 20 June 2019; Accepted 11 July 2019
Available online 12 July 2019
0939-6411/

(SimulationsPlus) the surface solubility is not accounted for. In addition, in all commercial platforms, the size of the Unstirred Water Layer (UWL) around the dissolving particles is considered equivalent for the free and micelle bound drug, when it should depend on the diffusion coefficient of the species [4]. Consideration of bulk solubility as the driver of dissolution rate ignores literature in this field which points to a different situation since the pioneering work of Higuchi on reactive surfaces [5]. When solutes, which diffuse out of a solid surface during dissolution, react with medium components, for example through an acid-base reaction, the local pH near the solid surface is different from that of the bulk. The dissolution rate of the solid depends in this case, on the surface drug solubility determined by the surface pH, and on the diffusion coefficients of all the species present. Several authors [6–10] have solved equations to calculate surface pH, species concentration profiles in the UWL, and ultimately dissolution rates for different scenarios as a function of bulk pH and of the properties and concentrations of buffers. For polyprotic bases reacting with polyprotic acids with certain combinations of p*K*as, the equations cannot be algebraically solved but approximations can be made depending on the predominant species or stepwise numerical solutions to these equations can be put in place. Due to the complexity of the equations and the numbers of ions to consider in the UWL, only one PBPK platform to our knowledge, GCoas v1.1 (Process Systems Enterprise Ltd), has undertaken a full integration of these parameters to date using the same UWL thickness in the model. However, these factors cannot be ignored, since for instance, for a weak base, the pH residing at the surface could be considerably higher than that of the bulk pH leading to lower *in vitro* or *in vivo* dissolution rates than anticipated by the current models with bulk pH.

In this work, equations to calculate surface pH are proposed for monoprotic and diprotic bases and compared to classical approaches using drug and reactant diffusion coefficients [7,10]. The surface solubility is then used to predict the *in vitro* dissolution rate at various pH where the drug is ionized. In addition, contrary to the current models which assume a similar UWL for unbound drug and micelles, an equation which considers a different UWL thickness for the free and micelle-bound drug is tested. Finally, a batch specific product particle size distribution (P-PSD) is introduced, which is derived from *in vitro* dissolution data, and which can be integrated in PBPK platform mechanistic dissolution models, to predict *in vivo* exposure for different product batches. This P-PSD is used by the PBPK model as a "drug substance" particle size input, but it represents the product batch behavior and therefore comprises the effect of the formulation disintegration or capsule rupture, drug substance dispersion and wetting, and eventually drug dissolution. The purpose of this work is to test the ability of a batch P-PSD to be used across various dissolution media and simulate the dissolution in various conditions.

2. Materials and methods

2.1. Materials

0.1 N, 0.01 N and 0.001 N HCl media were prepared using appropriate dilutions from concentrated HCl (Sigma Aldrich). 50 mM pH 6.8 phosphate buffer was prepared using sodium phosphate monobasic (Sigma Aldrich) and sodium hydroxide (Sigma Aldrich). 50 mM pH 4.1 and 4.5 acetate buffers were prepared using sodium acetate trihydrate (Sigma Aldrich) and acetic acid (Sigma Aldrich). 100 mM pH 4.5 sodium citrate buffer was prepared using citric acid monohydrate (Sigma Aldrich) and sodium citrate dihydrate (Sigma Aldrich). 50 mM pH 2.5 phthalate buffer was produced using potassium hydrogen phthalate (Sigma Aldrich) and hydrochloric acid (Sigma Aldrich). Sodium dodecyl sulfate (Sigma Aldrich) was added as a surfactant during some experiments to the pH 6.8 phosphate buffer. Simulated gastric fluid (SGF) was prepared as per the USP using concentrated HCl (Sigma Aldrich) and sodium chloride (Sigma Aldrich), pepsin was excluded. Fasted state simulated intestinal fluid, version 2, (FaSSIF-V2) was prepared using sodium taurocholate hydrate (Sigma Aldrich), lecithin (Lipoid), sodium hydroxide (Sigma Aldrich), sodium phosphate (Sigma Aldrich) and sodium chloride (Sigma Aldrich). Note that the buffer from FaSSIF-V1 [12] is used internally for analytical reasons but with FaSSIF-V2 bile salt and lecithin levels. Four clinical batches of acalabrutinib 100 mg capsules were studied - W027180, L0505541, W026394 and L0505009. Acalabrutinib reference standard was sourced internally.

2.2. Physicochemical properties of acalabrutinib

Acalabrutinib is a BCS class II drug and shows the following biopharmaceutical properties: MW 465.5 g mol^{-1}, true density of 1.34 g/mL, p*K*as = 3.54 (B), 5.77(B), 12.1 (A), intrinsic solubility = 48 µg/mL at pH 8. The solubility in Fasted State Simulated Intestinal Fluid (FaSSIF v2) [11], and Fed State Simulated Intestinal Fluid (FeSSIF) [12] are 0.12 mg/mL (pH 6.5) and 0.67 mg/mL (pH 5) respectively. The particle size of drug substance batches entering in the composition of the drug product batches studies in this work were measured by laser diffraction according to a methodology described by Pepin et al. [30].

2.3. Surface solubility for acalabrutinib

2.3.1. Experimental

The surface pH of acalabrutinib slurries in the absence of buffers was measured in HCl solutions of different molarities and in phosphate buffer at pH 6.8 using the technique proposed by Serajuddin et al. [8]. Briefly, 1 g of drug substance was vortexed with 1 mL of dissolution medium and the pH measured. This process was repeated adding 1 mL medium aliquots until up to 14 mL. Solid particles were present at all stages of the experiment.

2.3.2. Theory

In the presence of strong acids, the two basic moieties of acalabrutinib can react with protons from the bulk leading to the following reaction at the surface.

$$B + H^+ \leftrightarrow BH^+ + H^+ \leftrightarrow BH_2^{2+} \quad (1)$$

We hypothesize, similar to other authors [6,7,10], that during the acid-base reaction, the dissolution rate of the free base in acidic conditions is rapid enough to ensure that the unionized drug concentration in the presence of solid drug substance is constant and equal to the intrinsic drug solubility.

We assume that the molarity of protonated bases is 0 at the start of the reaction and that, since solid drug is present throughout dissolution, the concentration of unionized drug remains constant at S_0, the intrinsic solubility.

Species	B	H^+	BH^+	BH_2^{2+}
T_0	S_0	10^{-pH_b}	0	0
T pseudo eq	S_0	$10^{-pH_b} - x - y$	$x - y$	y

Using the reaction pseudo-equilibrium condition, it comes that x, the moles of unionized base reacting with protons per liter of suspension and y the moles of single-protonated base reacting with protons per liter of suspension can be obtained from solving Eq. (2):

$$2Z^2 + Z \times \left(K_{a2} + \frac{K_{a1}K_{a2}}{S_0}\right) - \frac{K_{a1}K_{a2}}{S_0}10^{-pH_b} = 0 \quad (2)$$

Where Z is defined by Eq. (3), and x by Eq. (4).

$$Z = \sqrt{y\frac{K_{a1}K_{a2}}{S_0}} \quad (3)$$

$$x = 10^{-pH_b} - y - \sqrt{y\frac{K_{a1}K_{a2}}{S_0}} \quad (4)$$

The surface pH is obtained from Eq. (5).

$$pH_S = -\log(10^{-pH_b} - x - y) \quad (5)$$

At pH values close to the highest p*K*a, the hypothesis that the base dissolves fast to compensate the acid base reaction at the surface is violated. A correction factor in the form of $Log\left(\frac{S_T}{S_0}\right)$, where S_T is the total base solubility (cf. Eq. (6)) is applied to multiply the value of intrinsic solubility S_0 in the equations above only if $Log\left(\frac{S_T}{S_0}\right) < 1$. The full description of the set of equations used to calculate surface pH for diprotic and monoprotic bases, and comparison with published approaches using diffusion coefficients [7,10], are found in the supplementary materials.

The total solubility versus pH for acalabrutinib is calculated according to Eq. (6), valid for both bulk and surface pH conditions.

$$S_T = S_0 \times \left(1 + \frac{|H^+|}{K_{a1}} + \frac{|H^+|^2}{K_{a1}K_{a2}}\right) \quad (6)$$

2.4. Micelle size measurements

Micelle size measurement was performed on a Zetasizer Nano ZS (Malvern, UK). Samples of FaSSIF-V2 and FeSSIF were measured in disposable sizing cuvettes at a temperature of 25 °C using a viscosity value of 0.8872 cP, a dispersant refractive index of water of 1.330 and material refractive index of polystyrene latex of 1.59 as the absolute refractive index of the material was unknown. The measurement angle selected was the backscattering angle of 173°.

Micelle diameters for FaSSIF-V2 and FeSSIF were measured at 20.8 nm and 6.0 nm respectively. The value obtained for FeSSIF at 25 °C is not significantly different from the one measured by Okasaki et al. at 37 °C of 6.3 nm [13]. The values measured at room temperature for FaSSIF-V2 and FeSSIF, were considered adequate to represent micelle sizes at 37 °C.

2.5. In vitro dissolution and analysis

All dissolution experiments were performed in Sotax AT7 or Distek 2100 USP apparatus 2 (paddle). Medium volume was fixed to 900 mL. Paddle speed was varied between either 50 or 75 rpm. Samples were withdrawn at typical time points of 10, 15, 20, 30, 45 and 60 min. Samples were filtered immediately using 0.45 µm 25 mm PVDF syringe filters (Millipore) with the first 3 mL discarded to waste.

Dissolution samples were all analysed against an external reference standard using either an HPLC-UV or a standalone UV finish. UV analysis was performed using a UV–vis spectrometer (Agilent) at 236 nm with a 1 mm path length quartz cell. An Agilent 1100 fitted with a UV variable wavelength detector was used for HPLC analysis. Mobile phases of 10 mM ammonium acetate and acetonitrile were used with a gradient elution on a Phenomenx Ultracarb ODS, column (100 mm × 4.6 mm, 5 µm). Injection volume was 10 µL and a detection wavelength of 285 nm was used.

2.6. Modelling in vitro dissolution

An in-house Microsoft Excel® tool was developed to fit *in vitro* dissolution rates according to the film theory, i.e. controlled by the drug diffusion through a stagnant film layer surrounding the dissolving particle called the unstirred water layer (UWL) [13]. If a surfactant is used in the dissolution medium, f_u the fraction of free drug in the medium is given by:

$$f_u = \frac{C_u(t)}{C(t)} \quad (7)$$

where $C_u(t)$ is the unbound drug concentration at all times and C(t) the total drug concentration at all times. Equilibration is assumed to be instantaneous and so f_u is anticipated to be constant. Since all dissolution conditions where micelles were present were obtained at pH values where the drug is not ionized, the affinity of the drug to the surfactant forming micelles k_{aff}, is experimentally related to apparent solubility vs surfactant concentration (C_{surf}) by:

$$C(t) = C_u(t) + k_{aff} \times C_{surf} \quad (8)$$

or at equilibrium:

$$S_{app} = S_0 + k_{aff} \times C_{surf} \quad (9)$$

where S_{app} is the apparent solubility in the presence of micelles. A more complete equation should be used to fit solubility values obtained in conditions where the drug is ionized. For a diprotic base, this would be:

$$S_{app} = S_0 \times \left(1 + K_0 C_{surf} + \frac{|H^+|}{K_{a1}} \times (1 + K_+ C_{surf}) + \frac{|H^+|^2}{K_{a1}K_{a2}} \times (1 + K_{++} C_{surf})\right) \quad (10)$$

where K_0, K_+ and K_{++} are the partitioning coefficients between the aqueous phase and micelles for the unionized, singly protonated and doubly protonated species. Since in the dissolution conditions reported in this manuscript, the amount of protonated species (single or double) is negligible, this equation simplifies to $S_{app} = S_0 \times (1 + K_0 C_{surf})$, which means that the affinity constant derived above uses the reduced equation $k_{aff} = K_0 S_0$.

The Nernst-Brunner equation, which describes the variation of amount of undissolved drug dm_{solid} (kg) with time for a solid particle is modified to take into consideration the binding of drug to micelles and the diffusion coefficient of micelles and pure drug out of the unstirred water layer. This equation is close to the one developed by Gamsiz et al. [14] although the treatment of fraction drug unbound and thickness in UWL differ from the approach taken by these authors.

$$\frac{dm_{solid}}{dt} = -A(t) \times \left(f_u \times \frac{D_u}{h_u(t)} + \frac{1-f_u}{f_u} \times \frac{D_b}{h_b(t)}\right) \times (C_{S,u} - C_u(t)) \quad (11)$$

where A(t) (m^2) is the surface area of the particle at time t, D_u and D_b the diffusion coefficients of the unbound drug and micelle containing the drug respectively ($m^2\ s^{-1}$), and where $C_{S,u}$ is the unbound drug solubility at the surface of the drug crystal and C_u, the unbound drug concentration in the bulk ($kg\ m^{-3}$).

The thickness of the unstirred water layer (UWL) is calculated over time for the unbound drug and assumed equivalent to the particle radius for small particles as long as the particle radius is below 30 µm and 30 µm for particles ≥ 30 µm [15]. This approximation is currently used in dissolution models and is also available in GastroPlus [13]. Sugano has shown that the thickness of the UWL would be closer to 20 µm for large particles at 20 rpm in 1L medium in USP2 and that agitation would reduce this limiting thickness to 10 µm for 200 rpm [16]. As the dissolution proceeds, the particles shrink and this stagnant film layer will be reduced as well according to time.

The thickness of the UWL for the micelle-bound drug is calculated based from the diffusion coefficients of the free drug and the micelle-bound drug according to the following equation [4].

$$\frac{h_b}{h_u} = \sqrt[3]{\frac{D_b}{D_u}} \quad (12)$$

The free drug or micelle-bound drug diffusion coefficients D ($m^2\ s^{-1}$) are obtained from literature data or from the Stokes Einstein equation, assuming that the molecular shape is a sphere of radius r_h (m).

$$D = \frac{kT}{6\pi\eta r_h} \quad (13)$$

where $k = 1.3806504\ 10^{-23}$ ($J\ K^{-1}$) is the Boltzmann constant, T is the absolute temperature in kelvin, η (Pa s) is the kinematic viscosity of the solvent and r_h (m) is the hydrodynamic radius of the diffusing solute. The hydrodynamic radius of the solute can be estimated, assuming that

the molecular shape is a sphere and that the hydration of the solute is negligible, by the following equation

$$r_h = \sqrt[3]{\frac{3M_W \times 10^{-3}}{4\pi N_A \rho_S}} \quad (14)$$

where M_W is the molecular weight of the drug (g mol^{-1}), N_A = 6.02214179 10^{23} (mol^{-1}) is the Avogadro number and ρ_S is the drug true density in (kg m^{-3}). The effect of temperature for dissolution is accounted for by a change in the water viscosity.

For very small particles (in the nanosize range), the solubility is different than that of larger particles. The particle size and the interfacial tension between the solid particle and the solvent phase have to be considered with the use of the Kelvin equation.

$$C_r = C_\infty \times exp\left(\frac{2\gamma V_{molar}}{rRT}\right) \quad (15)$$

where C_r stands for the solubility of a drug particle of radius r (m). C_∞ is the solubility of the same drug with no curvature (or an infinite radius of curvature) at temperature T. Units for C_∞ and C_r are the same relevant concentration units. R = 8.314472 J K^{-1} mol^{-1} is the ideal gas constant, T (K) is the absolute temperature, γ (J m^{-2}) is the interfacial tension between the solid and the liquid and V_{molar} (m^3 mol^{-1}) is the molar volume of the drug.

For acalabrutinib, the particle size range fitted during this work was such that the application of the Kelvin equation to the model did not change the result of the simulations even with high interfacial tension. It was therefore not considered further in the simulation.

The internal Microsoft Excel® tool works by assigning a solid drug mass to a spherical particle size distribution of up to n = 10 bins. For each bin 'i' in the distribution, the initial particle radius $r_i(0)$ is described and associated to a fraction of the total mass to dissolve $m(r_i.\,0)$. The number of particles in each bin is assumed constant during all the dissolution, until they have completely dissolved, and given by:

$$n(r_i, 0) = \frac{m(r_i.0)}{\frac{4}{3}\pi(r_i(0))^3\rho_S} \quad (16)$$

where ρ_S (kg m^{-3}) is the material true density assuming a spherical particle size. At all times, the UWL thickness for the dissolving particles and the unbound drug is given by $h_u(t) = r(t)$ if $r(t) < 30$ µm or $h_u(t) = 30$ µm if $r(t) \geq 30$ µm. In each particle bin the mass of particles is reduced by integrating equation (9) over time. Particles are allowed to shrink, and the surface area of particles dissolving is calculated for each time point in each bin by:

$$A(t) = n(r_i, 0) \times 4\pi(r_i(t))^2 \quad (17)$$

With this internal Excel® tool, it is possible to derive a P-PSD from *in vitro* dissolution rates, which is unique for a drug product batch and represents the impact of drug substance particle size, but also formulation or process parameters which may influence dissolution.

In the above equations, the impact of bulk reactant species diffusion coefficient on the drug dissolution rate was neglected and it was assumed that local conditions at the surface of the drug together with the diffusion coefficient of the free drug or micelle-bound drug would drive the dissolution rate. This choice was driven by use of GastroPlus™ as the PBPK platform used in the prediction of human pharmacokinetic profiles for acalabrutinib [30], since this software currently neglects the impact of bulk constituents for mechanistic drug dissolution.

For acalabrutinib, since at pH 6.8 the molecule is unionized and the surface solubility is equal to the bulk solubility, the dissolution data obtained in this media has been used to derive the batch dependent P-PSD by fitting the 10 bin PSD to the measured data. In order to verify the adequacy of the theoretical model proposed above, the batch specific P-PSD was then used to simulate all other measured dissolution conditions. Several hypotheses were made in the use of the model and proposed inputs for simple micelle-free media or media with micelles as illustrated in Table 1.

Table 1
Hypotheses for model verification using P-PSD as an input.

	Simple media		Micelle containing media		
Model inputs	Hyp 1	Hyp 2	Hyp 3	Hyp 4	Hyp 5
Use of surface pH and surface solubility	YES	NO	YES	YES	NO
Use of bulk apparent solubility	NO	YES	NO	NO	YES
Effect of micelle considered (f_u, D_u, D_b)	NA	NA	YES	YES	NA
Different UWL thickness $h_{b(t)} < > h_{u(t)}$	NA	NA	YES	NO	NA
Effect of micelle neglected (f_u = 1, D_u only)	NA	NA	NO	NO	YES

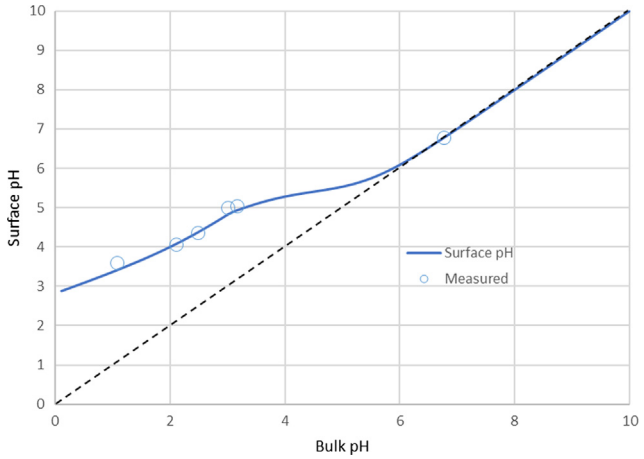

Fig. 1. Evolution of surface pH vs bulk pH for acalabrutinib.

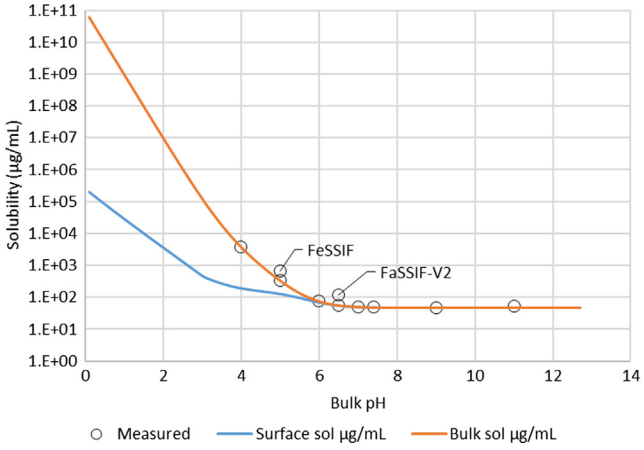

Fig. 2. Bulk and surface acalabrutinib solubility vs bulk pH.

The proposed theoretical approaches in this paper are Hyp 1 for prediction of dissolution rates measured in simple media, and Hyp 3 for prediction of dissolution rates measured in micelle-containing media. In addition to the verification proposed in Table 1, the drug substance full laser diffraction data was also used as an input to the model using Hyp1 and Hyp2 for simple media to check whether laser diffraction data on drug substance batches can provide a better prediction of *in vitro* dissolution of drug product than the approach of the P-PSD detailed in this work.

Table 2
Surface solubility in dissolution media used during study.

Medium	Surface solubility (mg/mL)
0.1 N HCl (bulk pH = 1)	29.2
SGF (bulk pH 1.2)	19.2
0.01 N HCl (bulk pH = 2)	3.73
pH 2.5 phthalate	1.34
0.001 N HCl (bulk pH = 3)	0.485
pH 4.1 acetate	0.187
pH 4.5 acetate	0.159
pH 4.5 citrate	0.159
Blank FaSSIF pH 6.5	0.0563
FaSSIF-V2 pH 6.5	0.12 ($S_{apparent}$) + 0.0563 ($S_{aqeuous}$)
pH 6.8 phosphate	0.0523
pH 6.8 phosphate + 0.2% SDS	0.62 ($S_{apparent}$) + 0.0523 ($S_{aqeuous}$)
pH 6.8 phosphate + 0.5% SDS	1.48 ($S_{apparent}$) + 0.0523 ($S_{aqeuous}$)

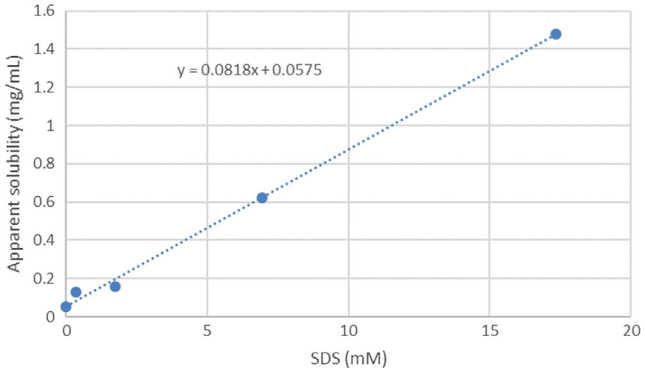

Fig. 3. Apparent acalabrutinib solubility as function of SDS concentration in pH 6.8 phosphate buffer.

Table 3
Particle size distribution of drug substance batches.

DP batch number	DS batch number	D(v,0.1) (μm)	D(v,0.5) (μm)	D(v,0.9) (μm)
W026394	FP-000180	233	313	392
W027180	FP-000221	131	235	394
L0505009	FP-000264	16	97.9	377
L0505541	FP-000298	47.1	225	345

2.7. Calculation of performance indicators for prediction of in vitro dissolution

In order to assess the model performance under the different hypotheses described above, the average fold error (AFE) and absolute average fold error (AAFE), were calculated for the prediction percent drug dissolved over all measured time points for each batch and each condition. The average fold error indicates whether the predicted values underestimate (less than one) or overestimate (more than one) the observed values. The absolute average fold error quantifies the absolute error for the prediction of the measured values.

$$AFE = 10^{\frac{1}{n}\times\sum Log\left(\frac{predicted}{observed}\right)} \quad (18)$$

$$AAFE = 10^{\frac{1}{n}\times\sum \left|Log\left(\frac{predicted}{observed}\right)\right|} \quad (19)$$

3. Results

3.1. Solubility

The measured surface pH and the calculated surface pH using the proposed theoretical method are presented in Fig. 1. The surface pH deviates from bulk pH below the highest basic p*K*a of acalabrutinib. At pH 1, there is a 2.5 pH unit difference between bulk and surface pH. It is not possible to measure the surface solubility of drugs, but it can be calculated from the surface pH and the pH solubility profile of the drug (equation (6)). The bulk and surface solubility of acalabrutinib are presented in Fig. 2 (see raw solubility data in Table S1). The surface solubility is considerably lower than the bulk solubility in acidic conditions with 4.5 log difference at pH 1, where the surface solubility of acalabrutinib is estimated to be 29 mg/mL.

The surface solubilities of acalabrutinib in the various dissolution media used during this work are presented in Table 2.

3.2. Additional inputs for micelle containing media

3.2.1. SDS

The apparent affinity of acalabrutinib to the SDS micelles is fitted to the surfactant concentration, using 1 h solubility data (Fig. 3). For acalabrutinib, this affinity is k_{aff} = 0.0818 mg/mL/mM SDS as shown in Fig. 3. The fraction of drug unbound in pH 6.8 phosphate buffer with SDS is calculated at 0.084 for 0.2% SDS and 0.036 at 0.5% SDS. The hydrodynamic radius of the SDS micelles used for 0.2% solution was 1.26 nm and 1.83 nm for 0.5% solution. They were calculated from the observed diffusion coefficients vs SDS concentration from Hammouda et al. [17] at 37 °C which were found comparable to data generated by

Table 4
Dissolution conditions studied, letters identify unique P-PSD and numbers identify media and conditions for dissolution data shown in Figs. 4–9.

Condition	Medium\Batch	L0505009		W026394		W027180		L0505541	
	Paddle Speed (rpm)	50	75	50	75	50	75	50	75
1	0.1 N HCl	A1	–	B1	–	C1	–	E1	–
2	SGF	A2	–	–	–	–	–	E2	–
3	0.01 N HCl	–	–	B3a*	B3b*	C3	–	–	–
4	pH 2.5 phthalate	A4*	–	B4*	–	C4*	D4*	E4*	–
5	0.001 N HCl	–	A5*	–	B5*	C5	D5*	–	E5*
6	pH 4.1 acetate	–	A6*	–	–	–	–	–	E6
7	pH 4.5 acetate	–	A7	–	B7	C7*	D7	–	E7
8	pH 4.5 citrate	–	–	–	–	–	D8	–	–
9	FaSSIF-V2 pH 6.5	–	A9	–	B9	–	–	–	E9
0	pH 6.8 phosphate	–	A0	–	B0	C0	D0	–	E0
10	pH 6.8 phosphate + 0.2% SDS	–	–	–	–	C10*	D10*	–	–
11	pH 6.8 phosphate + 0.5% SDS	–	–	–	–	–	D11*	–	–

–: Not performed,
* Infinity spin (250 rpm) performed after 60 min sampling timepoint.

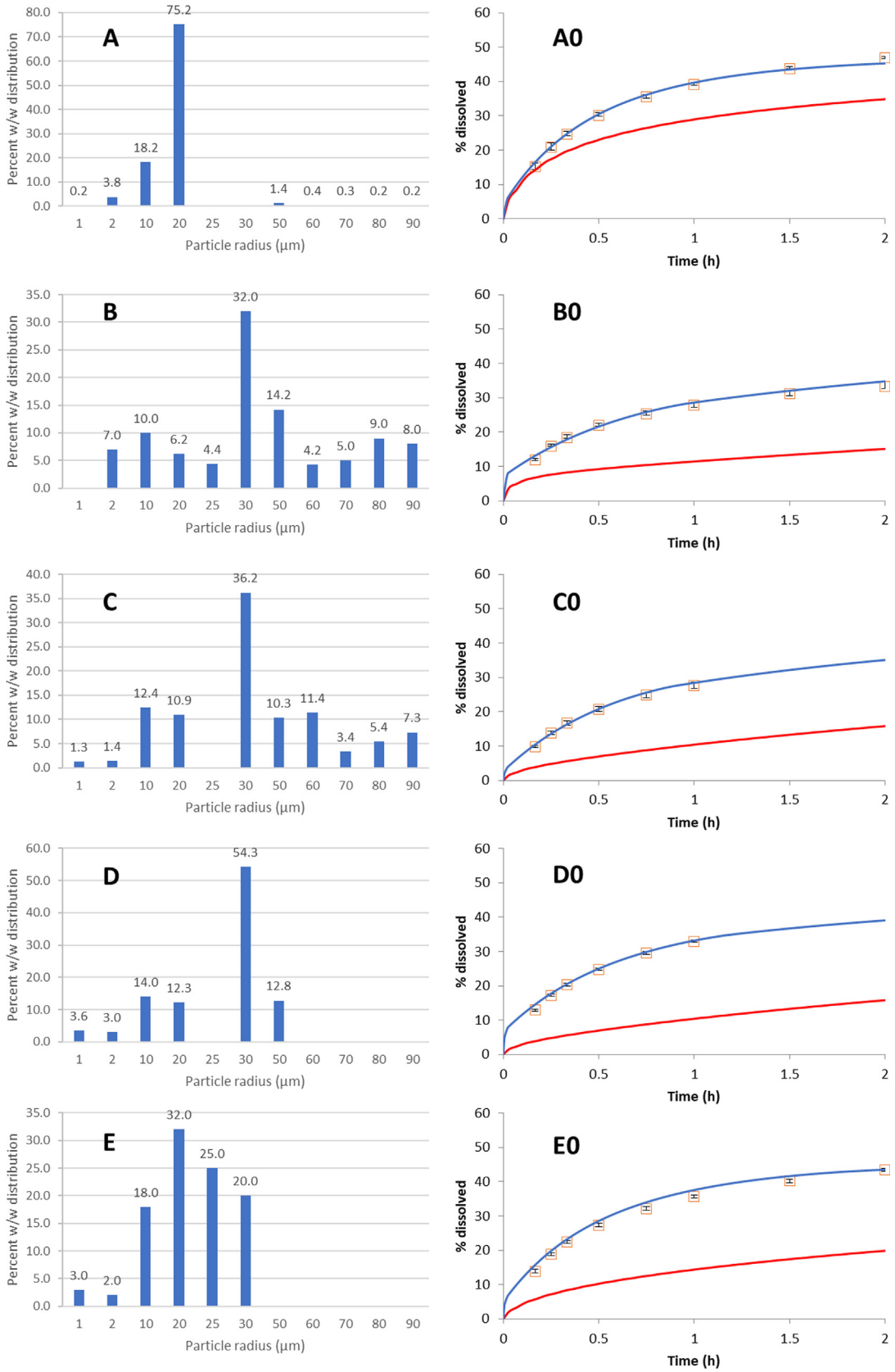

Fig. 4. P-PSD (left) extracted from pH 6.8 dissolution data (right) for batches: A = L0505009 at 75 rpm, B = W026394 at 75 rpm, C = W027180 at 50 rpm, D = W027180 at 75 rpm, and E = L0505541 at 75 rpm. Open symbols are measured data ± 1SD, solid blue lines are fitted profiles using surface (equal bulk) solubility, solid red line are predictions using laser PSD data for drug substances using surface (equal bulk) solubility. (For interpretation of the references to colour in this figure legend, the reader is referred to the web version of this article.)

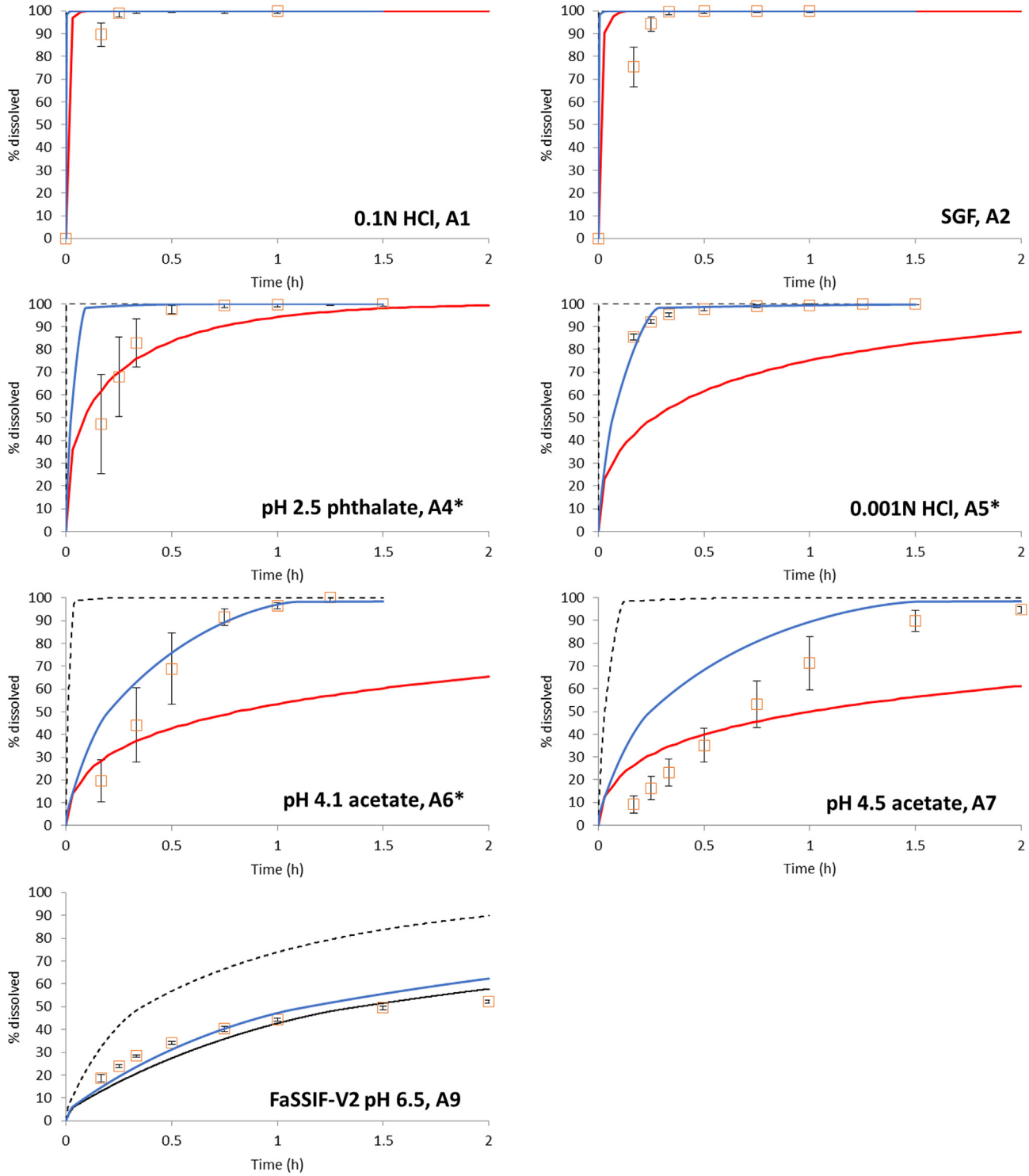

Fig. 5. Predicted dissolution rate for batch L0505009 with media as in Table 4. Dashed black line: bulk solubility, solid blue line: surface solubility, solid black line: same UWL thickness for micelle and free drug, solid red line: surface solubility and DS PSD. *: infinity spin from 60 min. (For interpretation of the references to colour in this figure legend, the reader is referred to the web version of this article.)

Clifford et al. [18] and Duplâtre et al. [19]. These hydrodynamic radii were used to calculate the diffusion coefficient of the drug bound in micelle using the Excel tool at 37 °C.

3.2.2. FaSSIF-V2

The apparent affinity of acalabrutinib to the sodium taurocholate micelles (k_{aff} = 0.0212 mg/mL/mM NaTC) is calculated using solubility values obtained in FaSSIF-V2 and water. The fraction of drug unbound in FaSSIF-V2 is 0.48. The diffusion coefficient selected for FaSSIF-V2 was taken as the lecithin measured diffusion coefficient, 0.5×10^{-10} m^2 s^{-1} as reported by Glanzer et al. [20]. These authors report a dissociation of lecithin and NaTC at this concentration. Note that using our own size measurements for FaSSIF-V2, the predicted diffusion coefficient value at 37 °C would be of 0.3 x 10^{-10} m^2 s^{-1} which does not impact significantly the predictions.

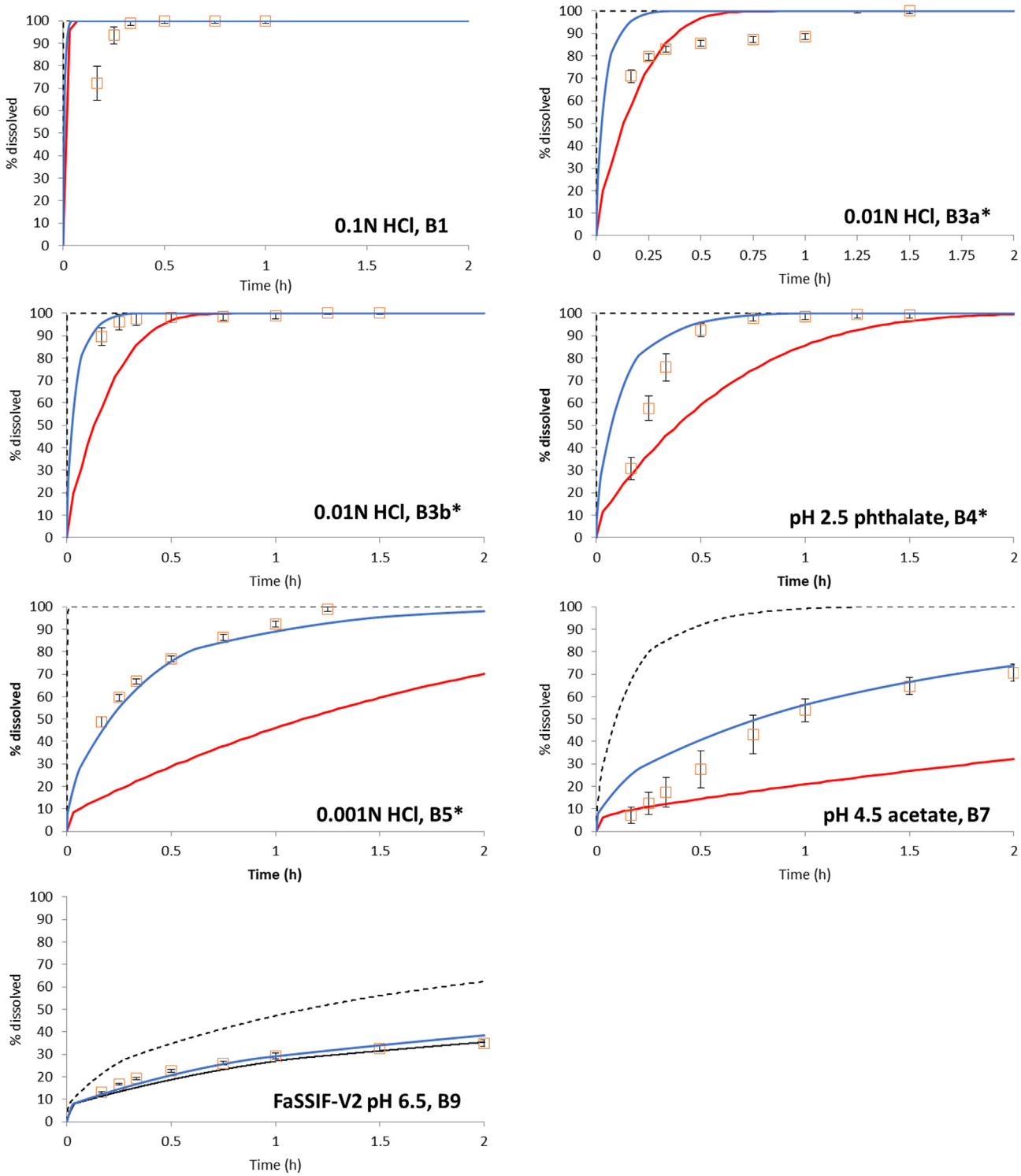

Fig. 6. Predicted dissolution rate for batch W026394 with media as in Table 4. Dashed black line: bulk solubility, solid blue line: surface solubility, solid black line: same UWL thickness for micelle and free drug, solid red line: surface solubility and DS PSD. *: infinity spin from 60 min. (For interpretation of the references to colour in this figure legend, the reader is referred to the web version of this article.)

3.3. Particle size distribution of drug substances

The particle diameter of drug substances comprised in the drug product batches studies in this work is reported in Table 3. The drug products can be ranked from containing the smallest to largest drug substances as follows: L0505009 < L0505541 < W027180 < W026394.

3.4. Dissolution

Table 4 shows the USP 2 dissolution testing conditions of the four clinical batches of acalabrutinib 100 mg capsules studied, which resulted from the dissolution method development work in support of the clinical program.

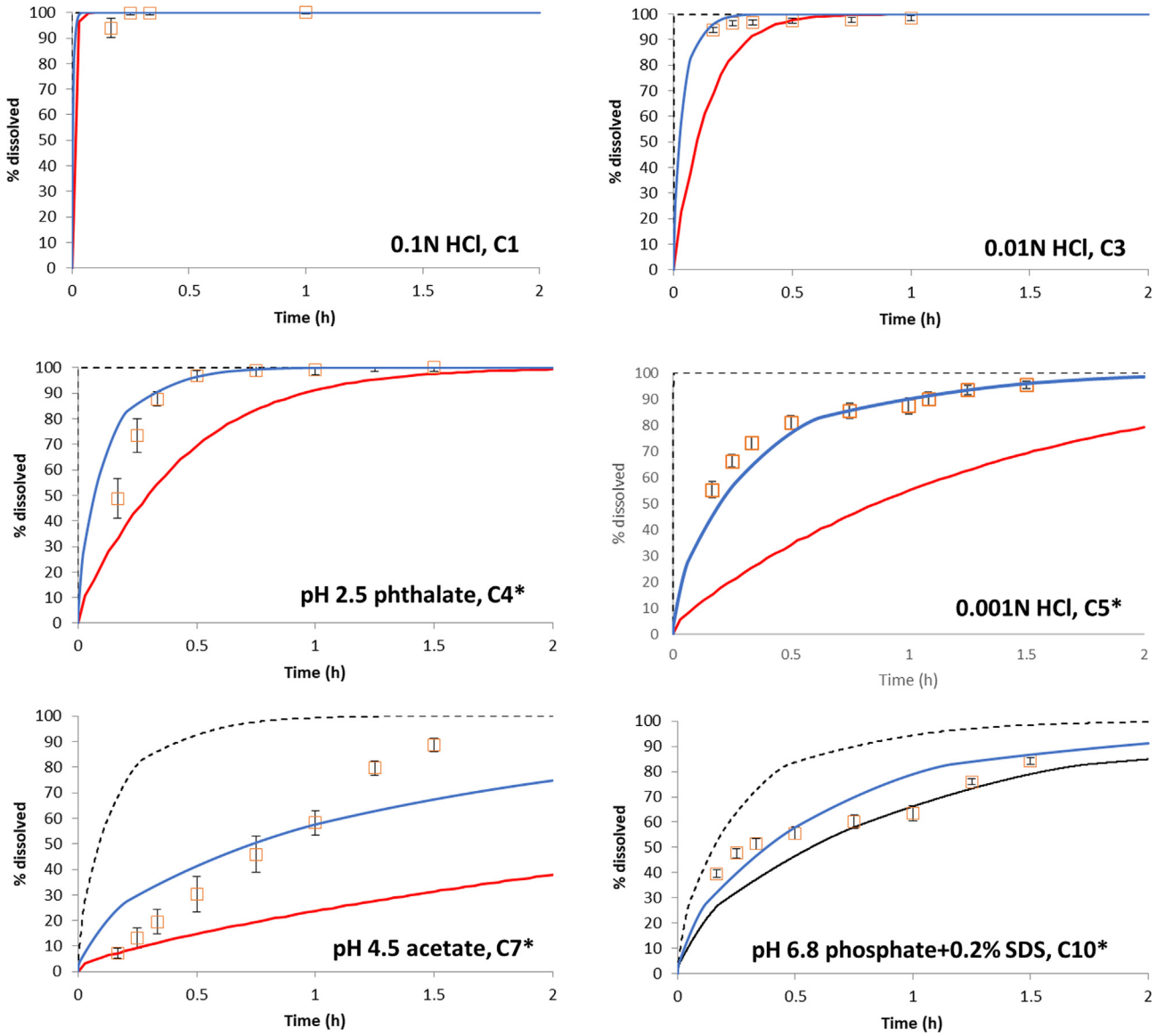

Fig. 7. Predicted dissolution rate for batch W027180 at 50 rpm with media as in Table 4. Dashed black line: bulk solubility, solid blue line: surface solubility, solid black line: same UWL thickness for micelle and free drug, solid red line: surface solubility and DS PSD. *: infinity spin from 60 min. (For interpretation of the references to colour in this figure legend, the reader is referred to the web version of this article.)

3.4.1. P-PSD fitting from in vitro dissolution and prediction from DS PSD

Dissolution data generated at pH 6.8 for the four batches were used to derive a P-PSD for each batch (Fig. 4). The drug products can be ranked according to their P-PSD from the smallest to the largest as follows: L0505009 < L0505541 < W027180 < W026394. P-PSD batch ranking corresponds to the drug substance particle size ranking, they are not anticipated to be strictly related, since P-PSD is derived from drug product dissolution, and comprises effects of excipients, manufacturing process, capsule rupture, and wettability of the drug substance.

3.4.2. Model verification with other dissolution conditions

Using the P-PSD extracted for each batch from pH 6.8 data (Fig. 4), the model was verified by its ability to predict the measured dissolution rate of these four batches in all other dissolution media tested, using the equations proposed in this paper and the hypothesis described in Table 1. In Figs. 5–9, the symbols and error bars represent measured data ± 1SD, the solid blue line is the proposed simulation strategy (Hyp 1 or 3), the dashed line is the prediction using bulk solubility (Hyp 2 or 5) and solid black line is the prediction for FaSSIF and SDS containing media, assuming the same UWL thickness for free and bound drug (Hyp 4). In addition, drug substance particle sizes obtained by laser diffraction were used to predict dissolution in simple media using surface solubility. These predictions are shown with solid red lines. All prediction performance indicators are calculated.

3.4.3. General discussion on prediction performance

The dissolution profiles of all acalabrutinib batches tested in this work are graphically well predicted in most media using Hyp1 and Hyp3 (the recommended approach), which rely on P-PSD, the surface solubility of acalabrutinib and, where relevant, the apparent total solubility in micellar media to calculate fraction unbound, and the micelle size using the methodology described in Section 3.6. In some cases, the rate is well predicted but there is a time lag between observed and predicted dissolution as for instance in media 1, 2, 4, 6, 7 or 8, but generally not in media containing surfactants like media 9, 10 or 11. This lag time could be explained by the wetting and dispersion time of the constituents or by the opening time of the gelatin capsule, which are measured *in vitro* but not predicted *in silico*.

The average AFE and AAFE for all the batches in media without

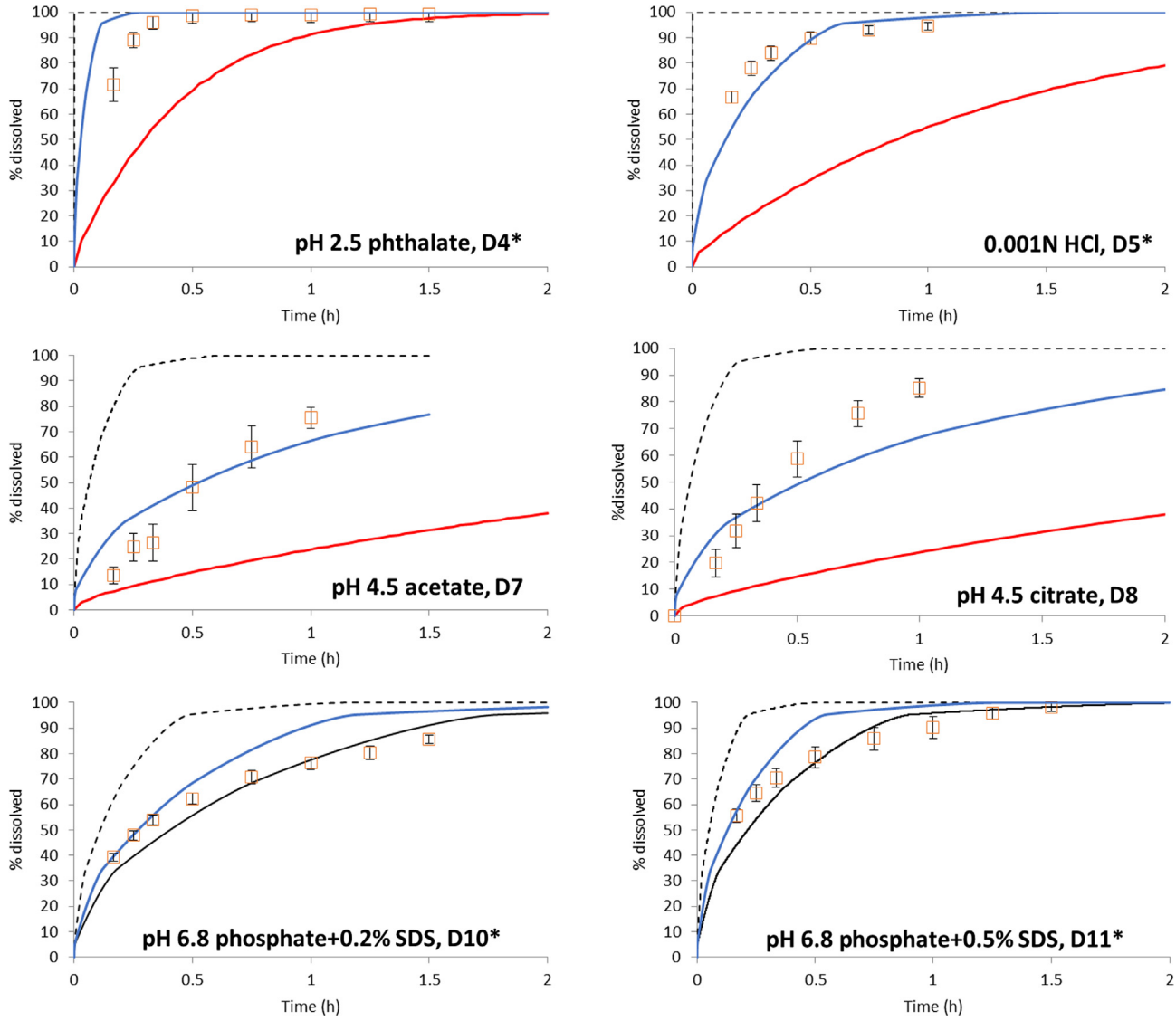

Fig. 8. Predicted dissolution rate for batch W027180 at 75 rpm with media as in Table 4. Dashed black line: bulk solubility, solid blue line: surface solubility, solid black line: same UWL thickness for micelle and free drug, solid red line: surface solubility and DS PSD. *: infinity spin from 60 min. (For interpretation of the references to colour in this figure legend, the reader is referred to the web version of this article.)

surfactants are presented in Figs. 10 and 11 respectively. Average prediction performance is calculated for each medium over all the batches tested and results are presented versus medium pH. The individual calculation of AFE and AAFE is found for each batch-medium combination in the Supplementary Table S2.

Several conclusions can be drawn from Figs. 10 and 11.

The use of bulk solubility and P-PSD (Hyp 2) overestimate the measured dissolution rate from pH values above 2. The maximal error in prediction is seen at pH 4.5 with an AFE of approximately 2.5 across all batches. Even if the difference between bulk and surface solubility is larger at the lowest pH (Fig. 2), the predicted and observed dissolution rates are very rapid below pH 2 regardless of whether bulk or surface solubility is used, which leads to limited prediction errors in both scenarios. As the pH increases, the solubility goes down and larger differences can be predicted depending on the hypotheses tested in this work. Over all conditions and batches tested, using bulk solubility leads to an overprediction and an absolute error of 48%. This observation confirms that surface pH matters for weak bases such as acalabrutinib, and that surface solubility should be included in the simulation of dissolution *in vitro* and *in silico*. Current PBPK models do not propose this calculation for weak bases and this work illustrates the error made in using bulk pH solubility profiles to calculate the *in vivo* dissolution of these drugs.

The use of DS PSD laser diffraction data as an input to the model is also clearly leading to 2-fold underprediction of observed dissolution rates from pH 3 to pH 6.8 (Fig. 10). Over all the conditions tested, the underprediction with DS PSD as an input is of 31% with an absolute error of 80%. Below pH 3, the error in prediction goes down as the medium becomes more acidic, since the solubility increases at low pH values cancelling differences in prediction. Since drug substances are generally non-spherical and may be aggregated, the surface area calculated from DS laser diffraction particle size data is always a low estimate of the true drug surface area available for dissolution. Laser diffraction data of the drug substance cannot be used directly to predict product performance [30].

Finally, the use of P-PSD and surface solubility (Hyp 1) allows a relatively constant prediction performance with AFE and AAFE close to 1 from pH 1 to pH 4.5. At pH 4.5, an average AFE of 1.4 ± 0.3 was calculated for this approach which may be related to the specific issues related to the choice of buffer at that pH (see below). Over all conditions tested in simple media, the error made using P-PSD and surface solubility is a 14% overprediction with an absolute error of 18%. This

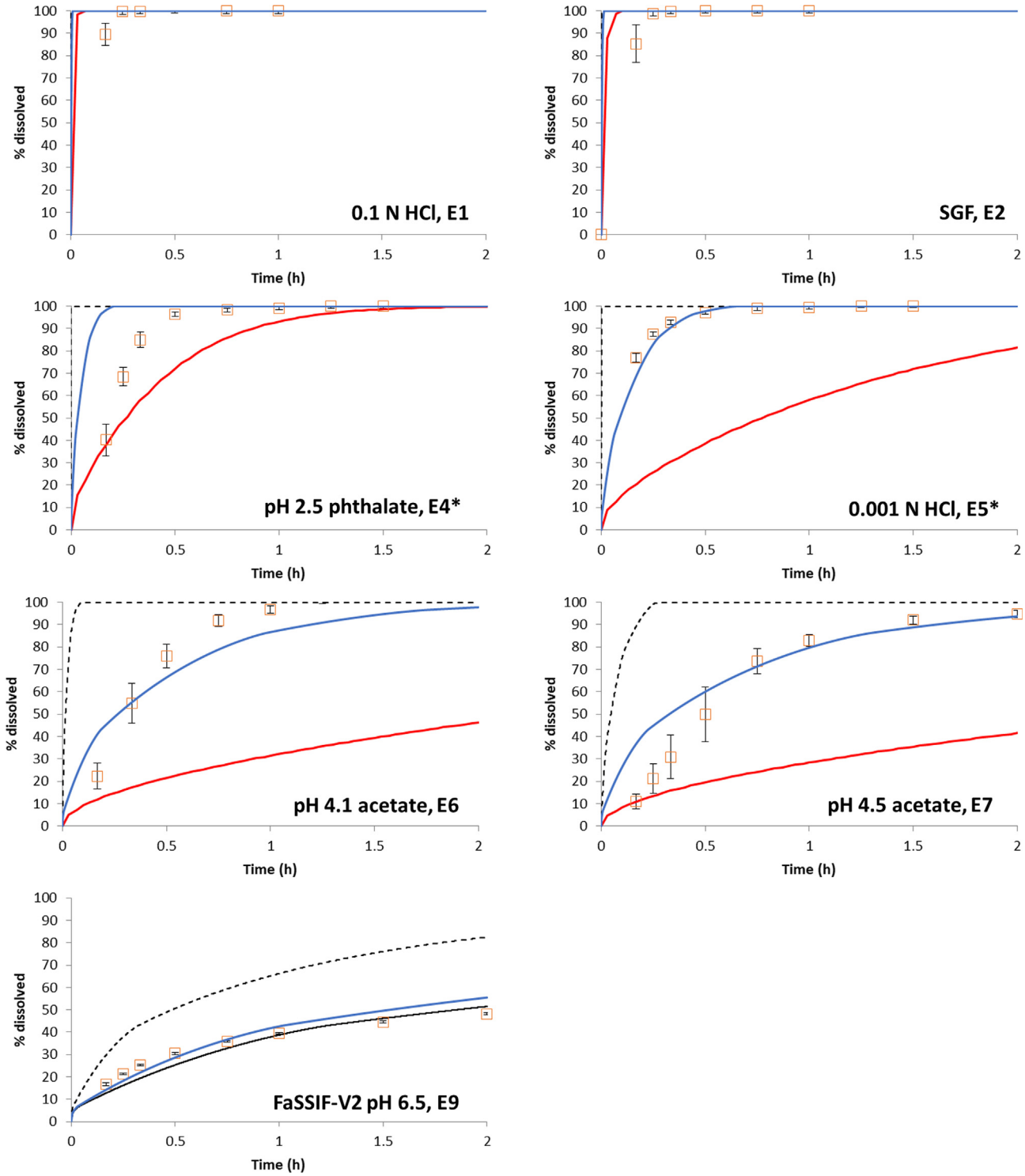

Fig. 9. Predicted dissolution rate for batch L0505541 with media as in Table 4. Dashed black line: bulk solubility, solid blue line: surface solubility, solid black line: same UWL thickness for micelle and free drug, solid red line: surface solubility and DS PSD. *: infinity spin from 60 min. (For interpretation of the references to colour in this figure legend, the reader is referred to the web version of this article.)

slight over-prediction could be related to opening times of capsules *in vitro* which is not accounted for *in silico*.

In more complex media like FaSSIF-V2 or SDS solutions at different concentrations, the AFE across 6 different batches were calculated at 1.02 ± 0.06 for Hypothesis 3 (P-PSD + surface solubility + micelles + different UWL), 1.51 ± 0.18 for Hypothesis 4 (P-PSD + bulk solubility) and 0.89 ± 0.04 for Hypothesis 5 (P-PSD + surface solubility + micelles + same UWL). The absolute errors (AAFE) were of 1.11 for Hypothesis 3, 1.51 for Hypothesis 4 and 1.15 for Hypothesis 5. There was no difference in prediction ability between FaSSIF-V2 or SDS solutions. The individual values for AFE and AAFE are found in supplementary Table S3.

These AFE values show that the use of bulk solubility overestimates the percent dissolved by 50% for micelle containing media whereas the use of surface solubility, accounting for micelle partitioning and different UWL for the micelle and the drug leads to unbiased predictions of

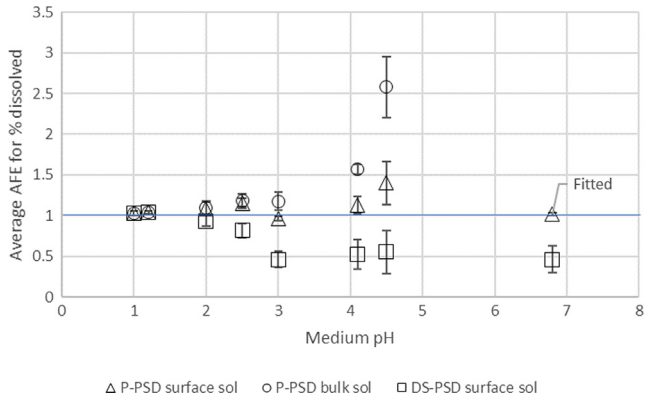

Fig. 10. Average AFE ± 1SD for all batches using simple media using Hyp1 (P-PSD and surface solubility), Hyp 2 (P-PSD and bulk solubility) or DS PSD and surface solubility.

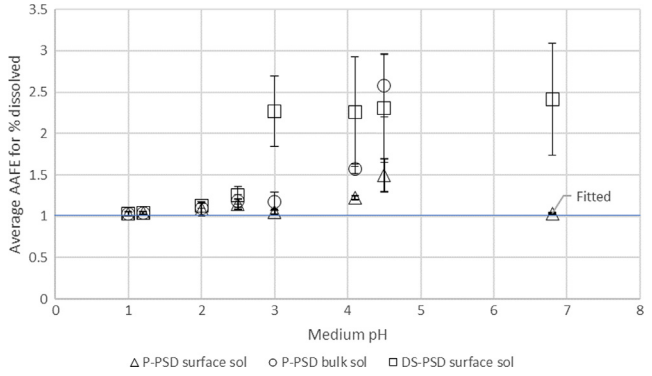

Fig. 11. Average AAFE ± 1SD for all batches using simple media using Hyp1 (P-PSD and surface solubility), Hyp 2 (P-PSD and bulk solubility) or DS PSD and surface solubility.

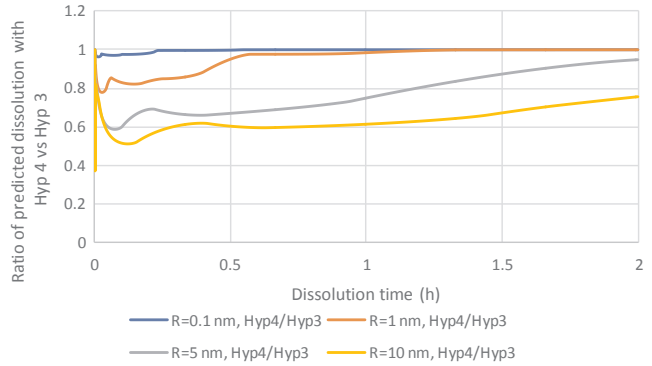

Fig. 12. Ratio of percent dissolved with Hyp 4 vs Hyp 3 for batch W027180 using various micelle sizes and solubility data and micelle concentration of experiment D11.

the dissolution rates. When the same UWL is hypothesized for free drug and micelle bound drug, there was a slight under-prediction of the dissolution data by approximately 10%.

Over all the media and batches tested, the recommended approaches (Hyp 1 or Hyp3) in this work allows to predict independent dissolution data with a slight over prediction of 11%. It is clearly the best of all strategies attempted for this drug.

3.4.4. Diffusion in the UWL

A batch P-PSD fitted at a typical agitation rate should normally include the effect of hydrodynamics on dissolution. However, since we have used a simple buffer at pH 6.8 where the drug is non-reactive, the P-PSD can only account for non-reactive drug diffusion and the diffusion of buffer constituents or reaction products during acid-base reaction at the surface is not considered in the model, whereas in reality, these may take time to diffuse and delay dissolution rate. With a higher agitation rate, these equilibria would happen more rapidly *in vitro*, moving the predictions closer to the measurements.

For the experiments conducted with citric acid or acetic acid in the buffer constituents (media 6, 7 or 8) the dissolution rates observed are more variable and show more or less pronounced linear portions at the beginning of dissolution. This is in contrast with all other observed media for the same batch. A potential explanation for the variability of dissolution at these pHs (4.1–4.5), is the proximity to acalabrutinib basic p*K*a values which could lead to variable solubility at the surface. Another explanation could lie in the nature (monoprotic or polyprotic), concentration and size of the buffer components used at that pH. Citric acid is expected to react twice with acalabrutinib in the 4.1–4.5 pH range, whereas acetic acid will react once. This could explain why batch W027180 dissolves faster in citrate medium compared to acetate medium, for the same bulk pH. The diffusion coefficient of hydronium ions is 10 times higher than most buffer constituents or drugs and within buffer constituents [21]. The diffusion coefficients of phosphoric [22,23] and acetic acid [24] are similar and approximately 30% higher than the diffusion coefficients of citric [25] and phthalic acids. These differences would be expected to play a role in limiting the dissolution rate of acalabrutinib in different media for equivalent buffer molar concentration and pH. Currently no PBPK model proposes a full description of the diffusion of reactants in the UWL during reactive dissolution. Since the objective of this work was to derive a batch-relevant input for GastroPlus™, we did not propose another model and hence restricted the diffusion coefficients to that of the free or drug bound to micelles which are handled by the software.

Integration of hydrodynamics *in vitro* and *in vivo* are important since the hydrodynamics *in vivo* are much slower than the ones typically applied *in vitro* in USP2, typically in the order of 20–75 rpm [16,26]. In addition, the food ingestion will alter the viscosity and hydrodynamics around immediate release dosage forms which may impact dissolution rate [3].

In addition, a more mechanistic understanding of the impact of buffer constituents on the *in vitro* dissolution of drug products will drive a better extrapolation in the calculation of *in vivo* dissolution since sodium bicarbonate, the physiological gastro-intestinal buffer, leads to different dissolution rates than the ones measured with phosphate buffers. For instance Krieg et al. [27] have shown how to calculate the impact of phosphate and bicarbonate on weak acid dissolution and how to adapt the concentration of phosphate buffers to get a more physiological dissolution rate depending on the drug pKa. If PBPK models were truly mechanistic for dissolution prediction and accounted for species reaction and diffusion, any buffer could be acceptable and used to gain more meaningful understanding of drug dissolution without the bias of buffer concentration and composition.

3.4.5. Thickness of the UWL

When simulating dissolution in media comprising micelles, we have tested in this work a hypothesis where the thickness of the UWL was different for the free and micelle-bound drug (Hyp 3). This is supported by literature data [4], but has rarely been applied to dissolution rate calculation using UWL models. The approach proposed by Crison et al. [28] uses a different thickness between free and micelle-bound drug, but the mass balance derivation for dissolution is different from the approach we propose. Gamiz et al. [29] or Okazaki et al. [13] do not consider a different thickness for UWL of the free or micelle-bound drug. In addition, simulations were run for media containing micelles with Hyp 4, which assumes identical UWL thickness for free and micelle-bound drug. Simulations run with Hyp 4 lead to lower predicted dissolution rates as expected from the mathematical description of the thickness ratio proposed by Pohl et al. [4].

The difference in prediction observed between using different or same UWL thicknesses is small and depends on the drug fraction unbound. For SDS micelles, the unbound drug fraction is in the order of 0.04 to 0.09 for acalabrutinib and the surfactant concentrations used and the effect of using the same or different UWL is more pronounced on these simulations compared to FaSSIF-V2 where the unbound drug fraction is of 0.48. For acalabrutinib in FaSSIF-V2, since the effect of changing the UWL thickness between free and micelle-bound drug is negligible, it was considered adequate to use the same UWL in GastroPlus. It is recommended to explore and integrate different UWL thicknesses in the *in vitro* and *in vivo* models to improve the prediction accuracy since this may be significant at different concentrations of micelles or for other drugs.

3.4.6. Other factors to consider

For the cases of B3a vs B3b, the underestimation of the dissolution extent for B3a compared to B3b likely resulted from a coning effect in the dissolution vessel at 50 rpm, leading to incomplete exposure to the dissolution medium. The data obtained with infinity spin after 1 h show rapid and complete dissolution of the drug (B3a*). Dissolution data obtained on the same batch at 75 rpm (B3b*) show a better agreement between prediction and measurement.

The size of micelles also influences the outcome of the simulations. Testing Hyp 4 (same UWL for free and micelle-bound drug) against Hyp 3 (different UWL for free and micelle-bound drug), it is apparent that the discrepancy between the two predictions will be dependent on the size of the micelles. With micelle size closer to the drug size, the two hypotheses lead to similar predictions of dissolution rate. For micelle sizes in the order of 10 nm hydrodynamic radius, the difference in predictions between Hyp 3 and Hyp 4 can be of at least 40% as illustrated for batch W027180 using solubility inputs and surfactant concentration from experiment D11 (Fig. 12).

4. General conclusions

The *in vitro* dissolution of acalabrutinib batches can be modelled using a batch specific P-PSD, which is a 10-bin particle size distribution based on measured dissolution rate in conditions where the drug is not reacting with buffer components. When acalabrutinib reacts with solutes from the bulk of the medium through acid-base reactions, the dissolution rate of acalabrutinib product batches depends on drug surface solubility determined by drug surface pH. Failing to acknowledge this, and using the bulk apparent drug solubility, leads to an overestimation of the drug dissolution rate at all pH values below the highest drug pKa. Since acalabrutinib exhibits two basic moieties, the adjustment of surface pH is not trivial, and can account, at pH 1, for up to 4.5 orders of magnitude difference between the bulk and the surface solubility. Between pH 2.5 and 5, the difference between predicted dissolution rate using bulk solubility or surface solubility is the largest for acalabrutinib, and the prediction error for the percent dissolution using bulk solubility can be as high as 250% at pH 4.5.

With the approach proposed in this work, the agreement between measurements and predictions is very good with an average overprediction of percent dissolution by 11% across all batches and conditions tested. This demonstrates that for immediate release products, the P-PSD can be used to reliably predict the drug product batch dissolution in different media spanning the physiological pH range and in the presence of synthetic or natural surfactants. In theory any dissolution method (whether devoid of surfactant, biorelevant or in the presence of a synthetic surfactant), could be used to derive the P-PSD for input in PBPK model, as long as the underlying mechanisms of the dissolution are well captured according to the methodology described in this work.

The equations to calculate surface pH for weak bases *in vitro* and *in vivo* are complex and have delayed the integration of surface pH calculation in PBPK platforms. However, GCoas v1.1 (Process Systems Enterprise Ltd) has managed this integration and Simcyp V17 proposes to calculate it for weak acids. This opens the way for broader application of these mechanistic models. The authors provide algebraic solutions to calculate surface pH for monoprotic and diprotic bases in in the supplementary materials and show how they fit measured surface pH for a variety of weak bases. In the absence of such calculation by the PBPK platform, it is recommended to alter the default pH in the relevant gastro-intestinal compartments, to reflect the surface pH of the drug of interest.

The size of micelles and the calculation of UWL thicknesses in different media could be easily implemented in all PBPK models, together with the equations for surface pH. This would greatly improve the prediction ability of the *in vivo* dissolution of weak bases where the effect of various pH conditions and bile salt concentrations could be more adequately reproduced. For acalabrutinib, since the same UWL in FaSSIF-V2 lead to the similar prediction errors compared to different UWL, the use of P-PSD was considered adequate in a PBPK platform. The companion paper [30] will show how the P-PSD for batches of acalabrutinib capsules administered in the clinic, allowed meaningful predictions of the observed human pharmacokinetics in various dosing conditions.

Appendix A. Supplementary material

Supplementary data to this article can be found online at https://doi.org/10.1016/j.ejpb.2019.07.014.

References

[1] A. Abend, et al., Dissolution and translational modeling strategies enabling patient-centric drug product development: the M-CERSI Workshop Summary Report, AAPS J. 20 (3) (2018).
[2] X.J. Pepin, et al., Justification of drug product dissolution rate and drug substance particle size specifications based on absorption PBPK modeling for Lesinurad Immediate Release Tablets, Mol. Pharm. 13 (9) (2016) 3256–3269.
[3] S. Cvijic, J. Parojcic, P. Langguth, Viscosity-mediated negative food effect on oral absorption of poorly-permeable drugs with an absorption window in the proximal intestine: In vitro experimental simulation and computational verification, Eur. J. Pharm. Sci. 61 (2014) 40–53.
[4] P. Pohl, S.M. Saparov, Y.N. Antonenko, The size of the unstirred layer as a function of the solute diffusion coefficient, Biophys. J. 75 (3) (1998) 1403–1409.
[5] W.I.P. Higuchi, E.L., D.E. Wurster, T. Higuchi, Investigation of drug release from solids II. Theoretical and experimental study of influences of bases and buffers on rates of dissolution of acidic solids. J. Am. Pharmaceut. Assoc. Am. Pharmaceut. Assoc., 67 (1958) (5), pp. 376–383.
[6] K.G. Mooney, et al., Dissolution kinetics of carboxylic acids II: effect of buffers, J. Pharmaceut. Sci. 70 (1) (1981) 22–32.
[7] K.G. Mooney, et al., Dissolution kinetics of carboxylic acids I: effect of pH under unbuffered conditions, J. Pharmaceut. Sci. 70 (1) (1981) 13–22.
[8] A.T.M. Serajuddin, C.I. Jarowski, Effect of diffusion layer pH and solubility on the dissolution rate of pharmaceutical bases and their hydrochloride salts I: phenazopyridine, J. Pharmaceut. Sci. 74 (2) (1985) 142–147.
[9] A.T.M. Serajuddin, C.I. Jarowski, Effect of diffusion layer pH and solubility on the dissolution rate of pharmaceutical acids and their sodium salts II: salicylic acid, theophylline, and benzoic acid, J. Pharmaceut. Sci. 74 (2) (1985) 148–154.
[10] S.S. Ozturk, B.O. Palsson, J.B. Dressman, Dissolution of ionizable drugs in buffered and unbuffered solutions, Pharmaceut. Res. 5 (5) (1988) 272–282.
[11] E. Jantratid, et al., Dissolution media simulating conditions in the proximal human gastrointestinal tract: an update, Pharm. Res. 25 (7) (2008) 1663–1676.
[12] E. Galia, et al., Evaluation of various dissolution media for predicting in vivo performance of class I and II drugs, Pharmaceut. Res. 15 (5) (1998) 698–705.
[13] A. Okazaki, T. Mano, K. Sugano, Theoretical dissolution model of poly-disperse drug particles in biorelevant media, J. Pharmaceut. Sci. 97 (5) (2008) 1843–1852.
[14] E.D. Gamsiz, et al., Predicting the effect of fed-state intestinal contents on drug dissolution, Pharmaceut. Res. 27 (12) (2010) 2646–2656.
[15] Y. Wang, et al., Comparison and analysis of theoretical models for diffusion-controlled dissolution, Mol. Pharmaceut. (2012) 120417094737002.
[16] K. Sugano, Theoretical comparison of hydrodynamic diffusion layer models used for dissolution simulation in drug discovery and development, Int. J. Pharmaceut. 363 (1–2) (2008) 73–77.
[17] B. Hammouda, Temperature effect on the nanostructure of SDS micelles in water, J. Res. Natl. Inst. Stand. Technol. 118 (2013) 151–167.
[18] J. Clifford, B.A. Pethica, The self-diffusion coefficient of sodium dodecyl sulfate micelles, J. Phys. Chem. 70 (10) (1966) 3345–3346.
[19] G. Duplâtre, M.F. Ferreira Marques, M. da Graça Miguel, Size of sodium dodecyl sulfate micelles in aqueous solutions as studied by positron annihilation lifetime spectroscopy, J. Phys. Chem., 100 (1996) (41), pp. 16608–16612.
[20] S. Glanzer, et al., Structural and functional implications of the interaction between

macrolide antibiotics and bile acids, Chemistry (Weinheim an Der Bergstrasse, Germany) 21 (11) (2015) 4350–4358.
[21] S.H. Lee, J.C. Rasaiah, Proton transfer and the mobilities of the H+ and OH- ions from studies of a dissociating model for water, J. Chem. Phys. 135 (12) (2011) 124505.
[22] F. Ruiz-Beviá, J. Fernández-Sempere, N. Boluda-Botella, Variation of phosphoric acid diffusion coefficient with concentration, AIChE J. 41 (1) (1995) 185–189.
[23] O.W. Edwards, E.O. Huffman, Diffusion of aqueous solutions of phosphoric acid at 25°, J. Phys. Chem. 63 (11) (1959) 1830–1833.
[24] V. Vitagliano, P.A. Lyons, Diffusion in aqueous acetic acid solutions, J. Am. Chem. Soc. 78 (18) (1956) 4538–4542.
[25] G.T.A. Muller, R.H. Stokes, The mobility of the undissociated citric acid molecule in aqueous solution, Trans. Faraday Soc. 53 (1957) 642.
[26] A. Scholz, et al., Can the USP paddle method be used to represent in-vivo hydrodynamics? J. Pharm. Pharmacol. 55 (4) (2003) 443–451.
[27] B.J. Krieg, et al., In vivo predictive dissolution: comparing the effect of bicarbonate and phosphate buffer on the dissolution of weak acids and weak bases, J. Pharmaceut. Sci. 104 (9) (2015) 2894–2904.
[28] J.R. Crison, et al., Drug dissolution into micellar solutions: development of a convective diffusion model and comparison to the film equilibrium model with application to surfactant-facilitated dissolution of carbamazepine, J. Pharmaceut. Sci. 85 (9) (1996) 1005–1011.
[29] R. Cristofoletti, N. Patel, J.B. Dressman, Assessment of bioequivalence of weak base formulations under various dosing conditions using physiologically based pharmacokinetic simulations in virtual populations. case examples: ketoconazole and posaconazole, J. Pharm. Sci. 106 (2) (2017) 560–569.
[30] X.J.H. Pepin, A.J. Moir, J.C. Mann, N.J. Sanderson, R. Barker, E. Meehan, A.P. Plumb, G.R. Bailey, D.S. Murphy, C.M. Krejsa, M.A. Andrew, T.G. Ingallinera, J. Greg Slatter, Bridging in vitro dissolution and in vivo exposure for acalabrutinib. Part II. A mechanistic PBPK model for IR formulation comparison, proton pump inhibitor drug interactions, and administration with acidic juices, Eur. J. Pharm. Biopharm. (2019), https://doi.org/10.1016/j.ejpb.2019.07.011.